RESEARCH ARTICLE | DECEMBER 04 2013

A method to control magnetism in individual strain-mediated magnetoelectric islands

Jizhai Cui (崔继斋); Joshua L. Hockel; Paul K. Nordeen; David M. Pisani; Cheng-yen Liang; Gregory P. Carman; Christopher S. Lynch

Appl. Phys. Lett. 103, 232905 (2013)
https://doi.org/10.1063/1.4838216

A method to control magnetism in individual strain-mediated magnetoelectric islands

Jizhai Cui (崔继斋), Joshua L. Hockel, Paul K. Nordeen, David M. Pisani, Cheng-yen Liang, Gregory P. Carman, and Christopher S. Lynch[a)]
Department of Mechanical and Aerospace Engineering, University of California, Los Angeles, California 90095, USA

(Received 17 August 2013; accepted 17 November 2013; published online 4 December 2013)

Patterned electrodes on a piezoelectric substrate are demonstrated to produce a localized strain of sufficient magnitude to control the magnetic anisotropy of a Ni island. Strain-induced magnetic anisotropy was measured using the magneto-optical Kerr effect, and the measured shifts in magnetic anisotropy were consistent with strain predicted using linear finite element analysis. This approach overcomes the effect of the substrate clamping the in-plane strain and should be scalable to thin films. This approach represents a key step toward realizing the next generation of strain mediated magneto-electric magnetic random access memory devices with low writing energy and high writing speed. © *2013 AIP Publishing LLC*. [http://dx.doi.org/10.1063/1.4838216]

Large strain-mediated magnetoelectric (ME) coupling can be obtained from composites comprising piezoelectric and magnetostrictive constituents arranged with various connectivities.[1] The underlying mechanism is a coupling between the piezoelectric and magnetostrictive effects. When the magnetoelectric composite consists of laminated thin layers of piezoelectric and magnetostrictive materials with the magnetization in the plane of the magnetic layer, an in-plane tensile strain component and an orthogonal in-plane compressive strain component will drive in-plane magnetization rotation. This has been observed in thin film Ni.[2,3] This strain state can be produced by a piezoelectric ceramic actuator using the sign difference between the piezoelectric coefficients d_{33} and d_{31}, and by certain anisotropic [011] cut and poled rhombohedral relaxor ferroelectric single crystals.[4] The magnetization is maintained in the plane of the film by the shape anisotropy. This approach has been used to tune ferromagnetic resonance (FMR),[5] induce magnetic coercive field changes,[6] and induce magnetization reorientation in magnetic thin film[2,7–10] and in small magnetic islands.[11,12] In the case of the islands, although the in-plane magnetization of the islands was rotated, all islands experienced the same strain and thus the magnetization of all islands rotated at once. Magnetic random access memory (MRAM) applications require a method to control individual magnetic islands,[13] the subject of the following discussion.

A linear piezoelectric finite element analysis (FEA) of small electrodes on the top surface of a thickness poled piezoelectric plate with the bottom side fully electroded was performed. The goal was to identify a geometry that overcomes the in-plane strain clamping effect that occurs when small electrodes are placed on a large piezoelectric plate or a thin piezoelectric film clamped by a substrate. The results indicated that when the electrode dimensions are comparable to the thickness of the piezoelectric plate, the out-of-plane (d_{33}) expansion and in-plane (d_{31}) contraction of the region beneath the electrodes produces a highly localized strain field. The strain fields interact when two such electrodes are separated by a distance of one to two times the plate thickness. This induces an in-plane bi-axial strain between the electrodes (tensile in one direction and contractile in the orthogonal direction). The piezoelectric coefficients and dimensions used in the simulations were $d_{33} = 690\,\text{pCN}^{-1}$ and $d_{31} = -340\,\text{pCN}^{-1}$, electrode dimensions $0.6 \times 0.6\,\text{mm}^2$, electrode separation distance 1.5 mm and 1.0 mm, plate thickness 0.5 mm, and applied potential 1.5 kV (nominal electric field $E_3 = 3\ \text{MVm}^{-1}$ beneath the small surface electrodes with the entire bottom surface at zero potential). Figure 1 shows the simulated bi-axial strain difference ($\Delta\varepsilon = \varepsilon_{xx} - \varepsilon_{yy}$) produced between the electrodes by the two electrode separation distances. Additional finite element simulations that included the conducting lines connected to the electrodes indicated a negligible effect on the strain field between the electrodes (not shown). Comparing Figs. 1(a) and 1(b), the bi-axial strain response in the piezoelectric material between the electrodes increases significantly as the electrode spacing approaches the thickness of the piezoelectric layer (roughly 680 ppm for L = 1.5 mm and 1100 ppm for L = 1.0 mm where L is the distance between the electrodes). Only a small region surrounding the electrodes is strained, thus enabling application to arrays of indexed magnetic elements.

Experiments were designed to verify that the localized strain field was generated between the electrodes. The experiments used a piezoelectric substrate with patterned electrodes arranged around a magnetostrictive island as shown in Figure 2. Ni was chosen for the islands as its response to bi-axial strain has been well characterized.[2,8,9,12] In this configuration, when a positive voltage is applied to one pair of top electrodes (either A-A or B-B) and the bottom surface is grounded as shown in Fig. 2(a), the piezoelectric material immediately under the electrodes expands out-of-plane (z-axis) and contracts in the x- and y-directions in-plane. Strain-displacement compatibility requires that the piezoelectric strain be compatible with the overall strain

[a)]Author to whom correspondence should be addressed. Electronic mail: cslynch@seas.ucla.edu

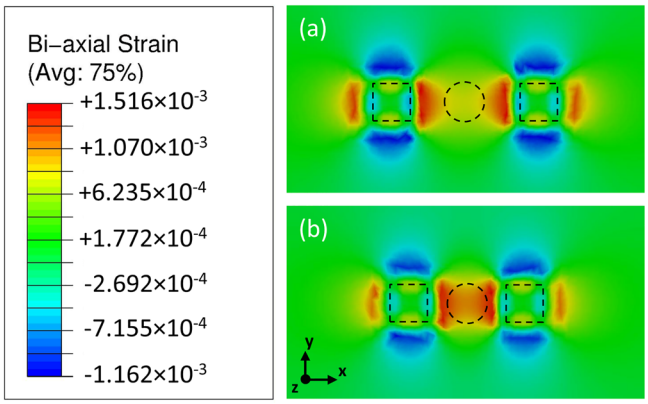

FIG. 1. Top view of FEA simulations of 1.5 kV applied to an electrode pair with the bottom surface at zero potential showing the bi-axial strain response ($\varepsilon_{xx} - \varepsilon_{yy}$) in the vicinity of an electrode pair with inter-pad spacing (a) L = 1.5 mm and (b) L = 1.0 mm. The dashed-line squares and circle indicate the location of the electrode pads and the magnetic element, respectively.

field. This induces a mechanical stretching of the material between the surface electrodes to accommodate the electric field induced in-plane contraction. When voltage is applied to electrodes A-A, the magnetic element is elongated along the x-direction ($\varepsilon_{xx} > 0$) and is contracted in the y-direction ($\varepsilon_{yy} < 0$). This combined action of elongation and contraction represents a local bi-axial strain difference in the region between the electrode pair, i.e., $\varepsilon_{xx} - \varepsilon_{yy} > 0$. The bi-axial strain between the electrodes is rotated 90° when voltage is applied to electrode pair B-B. This bi-axial strain difference

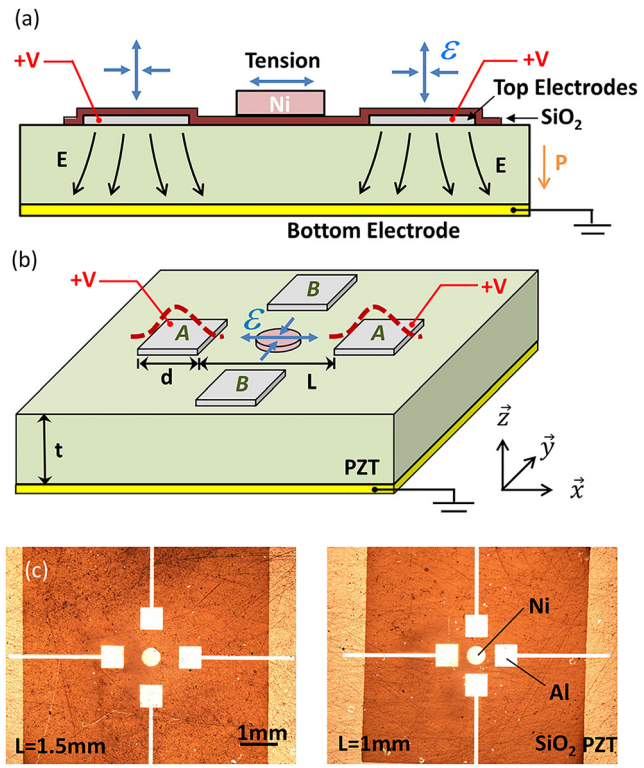

FIG. 2. Schematic of a device structure that generates localized bi-axial surface strain that interacts with a magnetostrictive element. (a) Cross section and (b) isometric view. The dashed line in (b) illustrates the out-of-plane expansion under the electrodes that creates the bi-axial strain field ($\varepsilon_{xx} - \varepsilon_{yy} > 0$) in the central Ni island. (c) Top views of fabricated patterned electrodes and Ni elements on PZT observed using an optical microscope.

$\Delta\varepsilon = \varepsilon_{xx} - \varepsilon_{yy}$ induces in-plane magnetoelastic anisotropy through the negative magnetostriction of Ni.

The configuration shown in Fig. 2 was fabricated on a polycrystalline plate of $Pb[Zr_xTi_{1-x}]O_3$ (PZT) with x approximately 0.52. A commercially obtained plate designated PZT-5H of dimensions $10 \times 10 \times 0.5\,mm^3$ was mechanically polished with 3 μm abrasive. The electrode patterns and magnetic Ni islands were deposited on the PZT plates using two-step optical mask lithography. As shown in Figs. 2(b) and 2(c), the electrode pads were $0.6 \times 0.6\,mm^2$ squares with inter-pad spacing of L = 1.5 mm or L = 1.0 mm. The small lines that connect to the pads were used for electric connection. Electrodes of 3 nm Ti (adhesion layer) and 100 nm Al were deposited by e-beam evaporation (CHA Solutions). 50 nm of SiO_2 was next evaporated to create an insulating layer to reduce the likelihood of electric breakdown between the pads. Finally, by the same technique a film of 3 nm Ti/35 nm Ni was deposited. The circular shape of the Ni was selected to minimize the effect of shape anisotropy in the multi-domain Ni that might directionally interfere with magnetization changes. The variation of the radius of the circular Ni element was less than 3% as measured from the optical micrographs. The uniformity of the Ni thickness was not measured. The SiO_2 insulation layer was used to screen charge, reducing the influence of any charge-induced ME effect on the measured magnetization change.[14,15] Formation of a nickel oxide surface layer can be avoided by deposition of a capping layer.[3,16] A capping layer was not used in this work. Ni has been studied as a capping layer for other magnetic thin films, and it was found that it takes 300 h in air to oxidize a 0.6 nm Ni layer.[17] The measurements reported here were performed within 300 h of processing, and an oxidation layer of <0.6 nm on the Ni should have little or no effect on magnetization measurements performed on a 35 nm Ni film. The Ni was e-beam evaporated and thus was not expected to have an initial easy axis such as that observed when Ni is magnetron sputtered; yet the experimental results indicate an initial bias in the M-H loops.

The electric field-induced magnetic anisotropy of the Ni was measured using longitudinal magneto-optical Kerr effect (MOKE) magnetometry. The magnetization of 35 nm thick Ni is in-plane due to the shape anisotropy.[2,18] The measurement direction of the Kerr rotation (i.e., the direction of the laser beam) was parallel to the direction of the applied magnetic field. The laser beam diameter was 0.5 mm which is the same as the diameter of the Ni disc; thus, the MOKE results represent the average magnetic response of the Ni disc. Figure 3 shows the normalized Kerr rotation hysteresis curves (M-H) for the electrode spacing case of L = 1.5 mm. Voltages of 0.5 kV, 1.0 kV, and 1.5 kV were applied to electrode pair A-A ($\varepsilon_{xx} - \varepsilon_{yy} > 0$) and then B-B ($\varepsilon_{xx} - \varepsilon_{yy} < 0$) during the MOKE measurement. For clarity, only the 1.5 kV case is shown.

Fig. 3(a) shows the magnetic response with H parallel to the x-axis, and Fig. 3(b) shows the magnetic response with H parallel to the y-axis. A comparison of the M-H loops prior to application of voltage to the electrodes (initial state) indicates the x-axis is a harder axis than the y-axis. Note the rounding of the M-H loop as the coercive field is approached in Fig. 3(a). The same loop in Fig. 3(b) with H parallel to the y-axis displays similar rounding at the bottom side of the

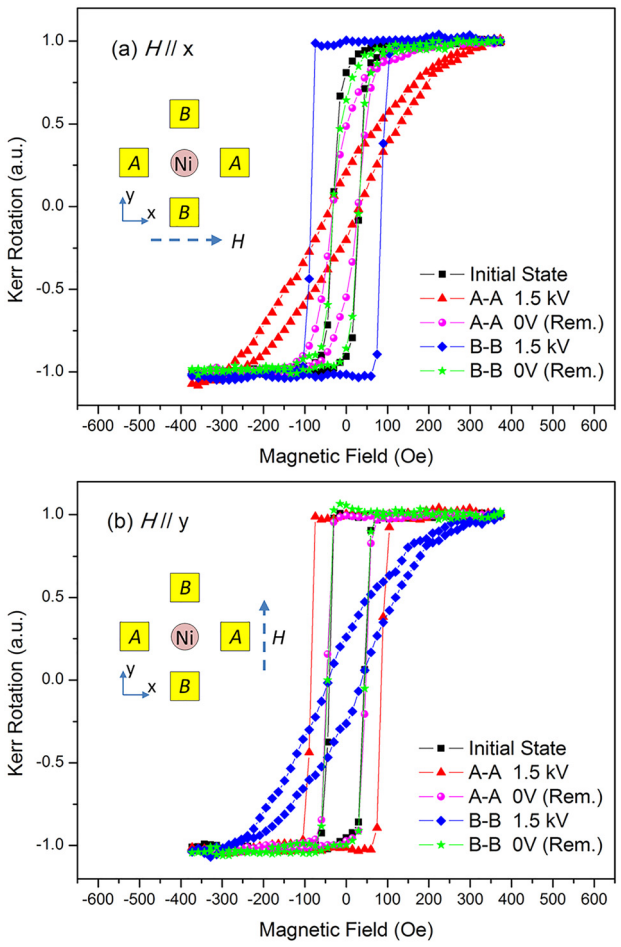

FIG. 3. Normalized Kerr rotation hysteresis curves (M-H) for L = 1.5 mm measured along (a) x-direction with magnetic field along x direction and (b) y-direction with magnetic field along y direction, under different applied voltages and for different electrode pairs.

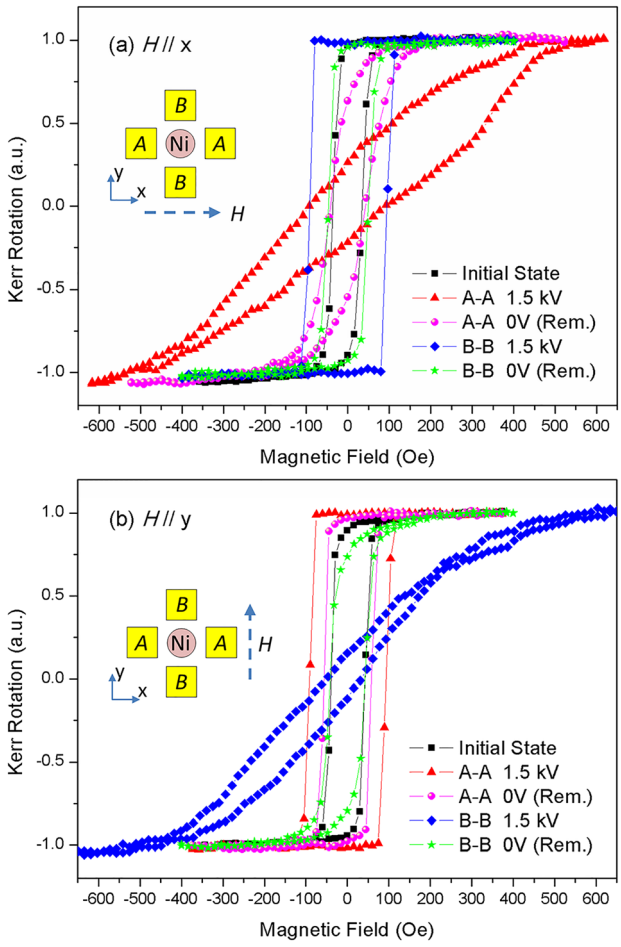

FIG. 4. Normalized Kerr rotation hysteresis curves (M-H) for L = 1 mm measured along (a) x-direction with magnetic field along x direction and (b) y-direction with magnetic field along y direction, under different applied voltages and for different electrode pairs.

loop and a sharper transition at the top of the loop. This effect is still present after the voltage cycles. Comparing with initial state, the loops change considerably when voltage is applied to electrode pair A-A. This is anticipated from previous work on Ni films.[2] In this case the strain component ε_{xx} is tensile and component ε_{yy} is compressive. "A-A 1.5 kV" in Fig. 3(a) indicates that a hard axis is induced in the x-direction while "A-A 1.5 kV" in Fig. 3(b) indicates an easy axis is induced in the y-direction. This is seen as the hysteresis loop becoming slanted to the right in Fig. 3(a) and requiring around 400 Oe to approach saturation, and as the hysteresis loop becoming much more square in Fig. 3(b). When the voltage is removed from electrode pair A-A as shown in "A-A 0 V (Rem.)" in Figs. 3(a) and 3(b), there is a residual hard axis in the x-direction and easy axis in the y-direction. This is likely the result of a change in the remnant strain state of the ferroelectric, an effect that cannot be predicted using a linear finite element analysis. When voltage is applied to electrode pair B-B ("B-B 1.5 kV" in Figs. 3(a) and 3(b)), the sign of the strain components is reversed, and the easy and hard axes invert, with the x-axis becoming the new easy axis and the y-axis becoming the new hard axis. The direction of the voltage-induced magnetoelastic anisotropy has been rotated 90° by removing the voltage from A-A and applying voltage to B-B.

The experiments were repeated with the electrode spacing reduced to 1 mm. This is the arrangement that produced a larger strain difference in the simulations. The results are shown in Figure 4. The initial state M-H curves, prior to application of voltage to the electrodes, display a slight asymmetry. When H is applied along the x-axis, there is slightly more rounding at the transition from negative to positive than at the transition from positive to negative. This suggests a preference for the magnetization to align in one direction over aligning 180° from that direction. This effect becomes considerably more pronounced when voltage is applied to electrode pair A-A, shown as "A-A 1.5 kV" in Fig. 4(a). When the electrodes are placed closer together, the magnetic field required to approach saturation in the hard axis direction is larger, around 600 Oe. The lack of symmetry in the M-H hysteresis loops is pronounced. Upon removal of the voltage from electrode pair A-A, there is a remnant hard axis in the x-direction and easy axis in the y-direction. The voltage sequence was switched from electrode pair A-A to pair B-B, and the magnetic anisotropy was again rotated 90°.

A previous study measured the response of thin film polycrystalline Ni to bi-axial strain.[2] That study included a discussion of the uniaxial degeneracy of the free energy induced by strain that gives rise to symmetric M-H hysteresis loops. The authors of that study pointed out that, based on

energy arguments, only the interaction of an applied magnetic field with the magnetization can break the symmetry of the M-H loops. In the experimental results presented above, the asymmetry of the M-H hysteresis loops suggests the presence of a bias magnetic field that was likely induced during processing. Several factors could be producing the initial easy axis, initial hard axis, and asymmetry in the M-H loops including magnetic domain pinning by the ferroelectric domains, irregularity in the shape of the circle, irregular edges in the circular pattern, strain gradients across the Ni, possibly thickness variations in the Ni film, and possibly a residual magnetization in the Ni sufficiently large that the results represent minor hysteresis loops with a lack of saturation in one direction.

The final goal of this work was to obtain an approximation of the strain from the observed changes in the M-H loops and to compare this to the strain predicted by the linear finite element simulation. To do this, the strain was approximated from the induced magnetic anisotropy. A measure of the anisotropy field H_a (the field needed to saturate the magnetization in the hard direction) was obtained using a linear fit to the slope of the M-H loops between −0.7 and 0.7. The average value of the slopes from each side of each hysteresis loop was extended from the origin to the saturation limit. Using the average reduced the effects of the asymmetry in the M-H loops. The intersection of this line and the $M/M_S = 1$(Kerr rotation) line was used as the estimated value of H_a. The same method was used to determine the saturation field H_0 in the initial state to provide both an x-axis and y-axis reference. The measured values of H_a were used to estimate the strain difference based on the known relationship between strain-induced magnetic anisotropy and bi-axial strain.

The equilibrium magnetization can be found from a minimization of the free energy[18] $E_{tot} = E_{zm} + E_{demag} + E_{ex} + E_{mc} + E_{me}$, where E_{zm} is the Zeeman energy, E_{demag} is the demagnetization energy, E_{ex} is the exchange energy, E_{mc} is the magneto-crystalline energy, and E_{me} is the magnetoelastic energy that represents the strain-induced magnetic anisotropy. For Ni thin film, assuming negligible in-plane shear strain and out-of-plane magnetization (i.e., $\varepsilon_{xy} = 0$ and $\alpha_3 = 0$),[19] the magnetoelastic energy is simplified to the uniaxial case as

$$E_{me} = B_1(\varepsilon_{xx} - \varepsilon_{yy})\alpha_1^2 \quad \text{for} \quad \varepsilon_{xx} - \varepsilon_{yy} > 0, \tag{1}$$

where α_i are the direction cosines of magnetization vector and ε_{ij} are the components of the magnetostrictive strain tensor; $B_1 = -(3/2)\ \lambda_S\ (C_{11}\text{-}C_{12})$ for polycrystalline Ni, $C_{11} = E(1-\nu)/[(1+\nu)(1-2\nu)]$ and $C_{12} = E\nu/[(1+\nu)(1-2\nu)]$, where λ_S is the magnetostriction constant,[18] E is the Young's modulus, and ν is Poisson's ratio. The constant terms that do not contribute to anisotropy were dropped. As $K_{me} = B_1(\varepsilon_{xx} - \varepsilon_{yy})$, this results in the expression

$$K_{me} = -\frac{3}{2}\lambda_S \frac{E}{1+\upsilon}(\varepsilon_{xx} - \varepsilon_{yy}). \tag{2}$$

The energy required to saturate the magnetization at zero strain is approximated as $E_0 = (1/2)H_0M_S$, where M_S is the saturation magnetization and H_0 is the field needed to saturate the magnetization. For $\varepsilon_{xx} - \varepsilon_{yy} > 0$, the total energy to saturate the magnetization is

$$E_{tot} = E_0 + E_{me} = E_0 + K_{me}\alpha_1^2, \tag{3}$$

where H_a is the anisotropy field along the hard axis and $E_{tot} = (1/2)H_aM_S$. Based on Eqs. (2) and (3) and $\alpha_1 = 1$ along the x-axis

$$(\varepsilon_{xx} - \varepsilon_{yy}) = \frac{-\Delta H_a M_S(1+\upsilon)}{3\lambda_S E}. \tag{4}$$

The material constants for polycrystalline Ni are E = 200 GPa, $\nu = 0.31$, $\lambda_S = -34 \times 10^{-6}$, and $M_S = 485$ emu/cc.[19]

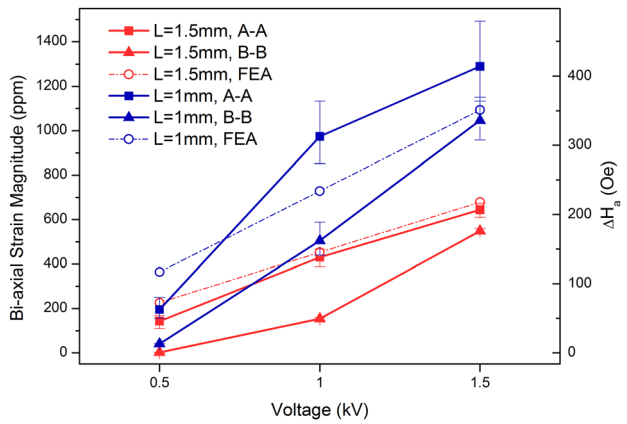

FIG. 5. Magnitude of bi-axial strain response (left ordinate) and ΔH_a along the hard axis (right ordinate) as a function of applied voltage for various electrode pairs and spacings. FEA simulations are indicated by the dotted-dashed lines.

Figure 5 is a comparison of the bi-axial strain under the Ni disc calculated using Eq. (4) with the FEA results. The error bars were obtained from the experimental results and represent the asymmetry of the hysteresis loops. Given that the magnetic analysis is first order and the finite element analysis neglects all non-linear effects, the agreement is remarkably good. This suggests that linear finite element analysis can be used as a design tool for patterned electrodes.

A method was developed that uses patterned electrodes on a piezoelectric substrate to generate a localized strain in a piezoelectric plate. This strain was used to control magnetic anisotropy in a 35 nm thick and 0.5 mm diameter Ni island. The bi-axial strain response was consistent with that predicted using linear piezoelectric FEA simulations. This method may be suitable for next generation MRAM devices with low writing energy and fast writing speed. This approach has the potential to be scaled down to the micro or nano-scale and used to achieve local in-plane strain on the surface of thin piezoelectric films subject to substrate clamping.

The authors would like to thank Scott Keller, Wen Dong, Sam Goljahi, and Dr. William T. J. McFinnister for their valuable discussions. This work was supported by NSF Nanosystems Engineering Research Center for Translational Applications of Nanoscale Multiferroic Systems (TANMS) Cooperative Agreement Award (No. EEC-1160504).

[1]C. W. Nan, M. I. Bichurin, S. X. Dong, D. Viehland, and G. Srinivasan, J. Appl. Phys. **103**(3), 031101 (2008).
[2]M. Weiler, A. Brandlmaier, S. Geprägs, M. Althammer, M. Opel, C. Bihler, H. Huebl, M. S. Brandt, R. Gross, and S. T. B. Goennenwein, New J. Phys. **11**(1), 013021 (2009).
[3]B. Özkaya, S. R. Saranu, S. Mohanan, and U. Herr, Phys. Status Solidi A **205**(8), 1876 (2008).
[4]T. Liu and C. S. Lynch, Acta Mater. **51**(2), 407 (2003).
[5]M. Liu, O. Obi, J. Lou, Y. J. Chen, Z. H. Cai, S. Stoute, M. Espanol, M. Lew, X. Situ, K. S. Ziemer, V. G. Harris, and N. X. Sun, Adv. Funct. Mater. **19**(11), 1826 (2009).
[6]J. Wang, J. Ma, Z. Li, Y. Shen, Y. Lin, and C. W. Nan, J. Appl. Phys. **110**(4), 043919 (2011).
[7]J. J. Yang, Y. G. Zhao, H. F. Tian, L. B. Luo, H. Y. Zhang, Y. J. He, and H. S. Luo, Appl. Phys. Lett. **94**(21), 212504 (2009).
[8]T. Wu, A. Bur, P. Zhao, K. P. Mohanchandra, K. Wong, K. L. Wang, C. S. Lynch, and G. P. Carman, Appl. Phys. Lett. **98**(1), 012504 (2011).
[9]T. Wu, A. Bur, W. Kin, Z. Ping, C. S. Lynch, P. K. Amiri, K. L. Wang, and G. P. Carman, Appl. Phys. Lett. **98**(26), 262504 (2011).
[10]Y. Dusch, N. Tiercelin, A. Klimov, S. Giordano, V. Preobrazhensky, and P. Pernod, J. Appl. Phys. **113**(17), 17C719 (2013).
[11]J. L. Hockel, A. Bur, T. Wu, K. P. Wetzlar, and G. P. Carman, Appl. Phys. Lett. **100**(2), 022401 (2012).
[12]M. Buzzi, R. V. Chopdekar, J. L. Hockel, A. Bur, T. Wu, N. Pilet, P. Warnicke, G. P. Carman, L. J. Heyderman, and F. Nolting, Phys. Rev. Lett. **111**(2), 027204 (2013).
[13]J.-M. Hu, Z. Li, L.-Q. Chen, and C.-W. Nan, Nat. Commun. **2**, 553 (2011).
[14]J.-M. Hu, C.-W. Nan, and L.-Q. Chen, Phys. Rev. B **83**(13), 134408 (2011).
[15]Z. Li, J. Hu, L. Shu, Y. Gao, Y. Shen, Y. Lin, and C. W. Nan, J. Appl. Phys. **111**(3), 033918 (2012).
[16]H. K. Kim, L. T. Schelhas, S. Keller, J. L. Hockel, S. H. Tolbert, and G. P. Carman, Nano Lett. **13**(3), 884 (2013).
[17]L. Gan, R. D. Gomez, C. J. Powell, R. D. McMichael, P. J. Chen, and J. W. F. Egelhoff, J. Appl. Phys. **93**(10), 8731 (2003).
[18]R. C. O'Handley, *Modern Magnetic Materials: Principles and Applications* (Wiley, New York, 2000).
[19]B. D. Cullity and C. D. Graham, *Introduction to Magnetic Materials* (IEEE-Wiley, Hoboken, NJ, 2009).